Transaction B: Mechanical Engineering
Vol. 16, No. 6, pp. 513–524

SCIENTIA IRANICA

Computational Simulation of Marangoni Convection Under Microgravity Condition

M.H. Saidi[1,*], M. Taeibi-Rahni[1,2], B. Asadi[1] and G. Ahmadi[3]

Abstract. *In this work, the rising of a single bubble in a quiescent liquid under microgravity condition was simulated. In addition to general studies of microgravity effects, the initiation of hydrodynamic convection, solely due to the variations of interface curvature (surface tension force) and thus the generation of shearing forces at the interfaces, was also studied. Then, the variation of surface tension due to the temperature gradient (Marangoni convection), which can initiate the onset of convection even in the absence of buoyancy, was studied. The related unsteady incompressible full Navier-Stokes equations were solved using a finite difference method with a structured staggered grid. The interface was tracked explicitly by connected marker points via a hybrid front capturing and tracking method. A one field approximation was used where one set of governing equations is only solved in the entire domain and different phases are treated as one fluid with variable physical properties, while the interfacial effects are accounted for by adding appropriate source terms to the governing equations. Also, a Multi-grid technique, in the context of the projection method, improved convergences and computational stiffness. The results show that the bubble moves in a straight path under microgravity condition, compared to the zigzag motion of bubbles in the presence of gravity. Also, in the absence of gravity, the variation of surface tension force due to interface curvature or temperature gradient can still cause the upward motion of the bubble. This phenomenon was explicitly shown in the results of this paper.*

Keywords: *Marangoni convection; Microgravity condition; Hybrid front capturing and tracking method; Rising bubble; Multi-grid method.*

INTRODUCTION

The variation of surface tension due to temperature gradient can initiate the onset of convection which is known as the common Marangoni convection. Note that, in the absence of temperature gradient, a variable surface tension force (not surface tension coefficient) may be generated due to the presence of surface curvature gradient. The variation of surface tension force can lead to a convective motion which is referred to as hydrodynamic convection.

The Marangoni convection is particularly important in the absence of buoyancy. It plays a crucial role in many applications, such as in crystal growth under microgravity condition, which is of interest to microelectronic industries. Understanding the thermo-capillary processes, especially the process of initiation of convection and when the flow become irregular, is very important for the corresponding manufacturing processes. Most earlier technological or scientific work performed under microgravity conditions was concerned with the improvement of the material processing procedures, while the fundamental fluid mechanics of the process is not fully understood. Another important application is the boiling heat transfer for enhancing the heat exchange processes under microgravity conditions. Again, the fundamentals of the microgravity boiling process are not fully understood. It is, therefore, important to have a thorough understanding of the process of bubble formation and motion under low gravity conditions where buoyant rise is negligible. Otherwise, understanding the physics of bubble motion under microgravity conditions is of great interest to a number of human life support applications in space.

1. *Center of Excellence in Energy Conversion, School of Mechanical Engineering, Sharif University of Technology, Tehran, P.O. Box 11155-9567, Iran.*
2. *Department of Aerospace Engineering, Sharif University of Technology, Tehran, P.O. Box 11155-9567, Iran.*
3. *Department of Mechanical and Aeronautical Engineering, Clarkson University, Potsdam, P.O. Box 13699-5725, NY, USA.*
*. *Corresponding author. E-mail: saman@sharif.edu*

Received 3 November 2008; received in revised form 3 March 2009; accepted 19 May 2009

In this work, the isothermal rising of a single bubble in a quiescent liquid under microgravity conditions was computationally investigated. The path of the bubble and the corresponding hydrodynamic Marangoni convection were evaluated. Note that the bubble was limited to a two-dimensional shape which is a severe approximation employed to allow reasonable resolution and computational requirements. However, such a formulation allows us to observe the sole effect of the bubble dynamics. In addition, the non-isothermal rising of a bubble was selected and Marangoni convection was studied in this paper.

For numerical simulation of the dynamics of large bubbles, the capturing and tracking of the interface is the most critical component. The computational results of Tryggvason et al. [1] have shown that the most accurate method for simulation of such flows is the hybrid front capturing and tracking technique. Although the efforts to compute multiphase flows are as old as Computational Fluid Dynamics (CFD), solving the full Navier-Stokes equations in the presence of a deforming interface has proven to be quite challenging. Only in recent years, major progress has been achieved with the use of the hybrid front capturing and front tracking method and also the level set method.

In addition to the hybrid front capturing and front tracking technique, several other techniques have been used in the past. A summary of the relevant techniques is provided here:

1. The oldest and still the most popular approach is to capture the interface directly on a regular and stationary grid. The MAC method in which marker particles are advected for each fluid particle, and the VOF method where a marker function is advected are the best known examples. In the earlier implementations of these techniques, the stress condition at the interfaces was satisfied rather crudely. However, a number of recent developments including a technique to include surface tension [2] and the use of "level sets" [3] to mark the fluid interface, has increased the accuracy of these techniques and thus their applicability.
2. The second class which potentially offers the highest accuracy uses separate boundary fitted grids for each phase. The steady rise of buoyant, deformable and axisymmetric bubbles was simulated by Ryskin and Leal [4] using this method. Using this approach, Dandy and Leal [5] also examined the steady motion of deformable axisymmetric droplets, while Kang and Leal [6] extended this methodology to axisymmetric unsteady bubble motion. The work of Leal et al. [4-6] had a major impact on subsequent research work in this area.
3. The third class is Lagrangian methods where the grid follows the fluid. Recent examples include two-dimensional computations of the break up of a droplet by Oran and Boris [7].
4. The fourth category is the front tracking method where a separate front marks the interface, but a fixed grid which is only modified near the front is used for the fluid within each phase. This technique has been extensively developed by Glimm [8].

As mentioned earlier, in this work we used the hybrid front capturing and front tracking method of Tryggvason et al. [1] which is a combination of front capturing and front tracking techniques. In this method, a stationary regular grid is used for the fluid flow, while the interface is tracked by a separate grid (front grid) that is embedded on the first one but moves with the interface. Note that, in the hybrid front capturing and front tracking method, all phases are treated by a single set of governing equations, while in the front tracking method, each phase is treated separately. This method was developed by Unverdi and Tryggvason [1,9]. Loth et al. [10-12] used this method to investigate the shear flow modulation and bubble dispersion of a bubbly mixing layer flow. Others also used this method to examine a number of other multiphase flow problems, e.g. the collision of two equal size droplets [13]. Another use of this method was the study of the breakup of accelerated droplets where both "bag" and "shear" breakup have been observed [14].

Multiphase flow computations involve coupled momentum, mass and energy transfer between moving and irregularly shaped boundaries, large property jumps between materials and computational stiffness. In this study, we focus on a combined Eulerian-Lagrangian method to investigate performance improvement using the multi-grid technique in the context of the projection method. The main emphasis was on the interplay between the multi-grid computation and the effect of the density ratios between phases. As the density ratio increases, the single grid computation becomes substantially more time-consuming; with the present problems, an increase of factor 10 in density ratio results in, approximately, a three-fold increase in CPU time. Overall, the multi-grid technique speeds up the computation and, furthermore, the impact of the density ratio on the CPU time required was substantially reduced [15-17].

IMPORTANT DIMENSIONLESS NUMBERS

The rise of a bubble in a quiescent liquid and its associated convection depend on the liquid physical properties, such as density, kinematic viscosity and surface tension. The most important physical dimensionless numbers in such a flow are: bubble Reynolds number, Re_B, Bond (Eotvos) number, Eo (Bo), Morton

number, Mo, Weber number, We, Marangoni number, Ma, and Froude number, Fr, defined, respectively, as:

$$\mathrm{Re}_B = \frac{2U_T r_{\mathrm{eq}}}{\nu}, \tag{1}$$

$$\mathrm{Eo\ (Bo)} = \frac{4\rho r_{\mathrm{eq}}^2 g}{\sigma}, \tag{2}$$

$$\mathrm{Mo} = \frac{g\nu^4\rho^3}{\sigma^3}, \tag{3}$$

$$\mathrm{We} = \frac{2\rho U_T^2 r_{\mathrm{eq}}}{\sigma}, \tag{4}$$

$$\mathrm{Ma} = \frac{\partial\sigma}{\partial T}\frac{\partial T}{\partial x}\frac{L^2}{\alpha\mu}, \tag{5}$$

$$\mathrm{Fr} = \frac{U_T^2}{2gr_{\mathrm{eq}}}. \tag{6}$$

Here, $r_{\mathrm{eq}} = \left(\frac{3V}{4\pi}\right)^{1/3}$ and ρ and ν are the density and the kinematic viscosity of the liquid, respectively. Note that the Morton number is related to the liquid physical properties and is independent of the flow conditions. Liquids can be categorized in different groups, namely those with high Morton numbers (Mo $> 10^{-2}$), those with intermediate Morton numbers and those with low Morton numbers (Mo $< 10^{-6}$). On the other hand, the Bond number characterizes the bubble size so that a functional relationship between any parameter and the Bond number describes how that parameter changes with the bubble volume. The terminal rise velocity of bubble (U_T) in Definition 1 is a function of equivalent radius, density, kinematic viscosity, gravitational acceleration and surface tension. Note that, in most practical applications, interest is mainly in low Morton numbers and moderate Reynolds numbers (between 200 and 900). At lower Reynolds numbers, however, bubbles have an approximately spherical shape, and they rise in a rectilinear path. Whereas, at intermediate and high Reynolds numbers, bubbles become oblate ellipsoids and rise in an irregular (zigzagging or spiraling) fashion. The summary of observed path and transition criteria at normal gravity is listed in Table 1 [18].

A flow induced by surface tension gradients or thermal gradients is termed Marangoni convection. For most fluids, the temperature gradient of surface tension $\left(\frac{\partial\sigma}{\partial T}\right)$ is negative and regions of higher temperature exhibit a reduced surface tension. Therefore, Marangoni convection, according to a Ma Number, results in a recirculating fluid flow from the warmer to the colder regions of a liquid and small temperature gradients give rise to relatively high fluid velocities along the phase boundary [19].

GOVERNING EQUATIONS

As noted before, in the hybrid front capturing and front tracking technique used here, only one set of governing equations is used for both phases, which requires accounting for the interfacial effects by adding the appropriate source terms to the governing equations [20,21]. Since the physical properties and the flow field are discontinuous across the interface, all variables must be interpreted in terms of generalized functions. Thus, various fluids can be identified by a step (Heaviside) function (H) which takes the value of one-for-one particular fluid and zero for the other. The interface is marked by a non-zero value of the gradient of the step function. It is most convenient to express H in terms of an integral over the product of one-dimensional δ-functions as follows:

$$H(x,y,t) = \int_A \delta(x-x^f)\delta(y-y^f)dA. \tag{7}$$

The density as well as any other physical properties can be written in terms of both the constant densities on either side of the interface and the above Heaviside

Table 1. Summary of some previous experimental results about bubble shape under normal gravity [18].

	Observed Shapes and Onset of Shape Instability		
	Spherical	**Ellipsoidal**	**Unstable**
Aybers & Tapucu (1969)	$r_{\mathrm{eq}} < 0.42$ mm	$r_{\mathrm{eq}} < 1.00$ mm	$r_{\mathrm{eq}} > 1.00$ mm
			We > 3.7
Haberman & Morton (1954)	Re < 400	$400 <$ Re < 5000	
Miksis et al. (1981)			We > 3.23
Ryskin & Leal (1984)	Contaminated liquids		Re > 200
	Pure liquids		We $> 3-4$
Duineveld (1994,1995)			We > 4.2
			$r_{\mathrm{eq}} > 1.34$ mm
Benjamin (1987)			We > 3.271

function as:

$$\rho(x,y,t) = \rho_i H(x,y,t) + \rho_o(1 - H(x,y,t)). \quad (8)$$

Here, ρ_i and ρ_o are the density at $H = 1$ and 0, respectively. On the other hand, for the viscous term, the full deformation rate tensor is implemented, while the conservative form of the advection term is normally used. Thus, the linear momentum equation is written as:

$$\frac{D(\rho u)}{Dt} = -\nabla P + \rho g + \nabla.\mu(\nabla u + \nabla^T u) + \sigma k n \delta(x - x^f). \quad (9)$$

Note that the surface tension forces have been added as a delta function which is non-zero only on the bubble surface where $x = x^f$. The interface force acting on the marker points is spread to the nearby grid points using the discrete Delta function defined as follows:

$$\delta(x - x_k) = \begin{cases} 0, & \text{otherwise} \\ \prod_{n=1}^{3} \frac{1}{d_p}\left(1 + \cos\frac{\pi(x-x^f)}{d_p}\right), & \text{if } |x-x^f| \le d_p \end{cases} \quad (10)$$

The mass conservation law is written as:

$$\frac{\partial \rho}{\partial t} + \nabla.\rho u = 0. \quad (11)$$

In this work, the flows of fluids are both assumed to be incompressible so that the density of a fluid particle in the flow field remains constant. Thus:

$$\frac{D\rho}{Dt} = 0, \quad (12)$$

and:

$$\nabla.u = 0. \quad (13)$$

The viscosity of each fluid particle is also assumed to be constant. Thus:

$$\frac{D\mu}{Dt} = 0. \quad (14)$$

The thermal energy equation with an interfacial source term to account for the liberation or absorption of latent heat is:

$$\frac{D(\rho c_p T)}{Dt} = \nabla.k'(\nabla T) + \dot{m}_f L \delta(x - x^f),$$
$$L = L_0 + (c_1 - c_2)T_{\text{sat}}. \quad (15)$$

Here, T is the temperature and L_0 is the latent heat measured at the equilibrium saturation, $T_{\text{sat}}(P)$, corresponding to the reference ambient system pressure [22].

NUMERICAL METHODOLOGY

In this work, the unsteady Navier-Stokes equations are solved using the finite difference method with a staggered fixed structured grid, while the interface (front) is tracked explicitly by connected marker points. The interfacial source term (surface tension effect) is computed at the front grid points and is interpolated on the fixed grid. The advection of fluid properties, such as density is accounted for by following the motion of the front. Figure 1 shows the fixed Eulerian and the moving Lagrangian grids used.

For solving the governing equations, the following points have to be accounted for:

- The density and the viscosity changes due to the phase transport.
- The surface tension effect is only at the front.
- Accurate evaluation of velocity and the pressure fields at each time step.
- Accurate evaluation of the motion of the interface itself.

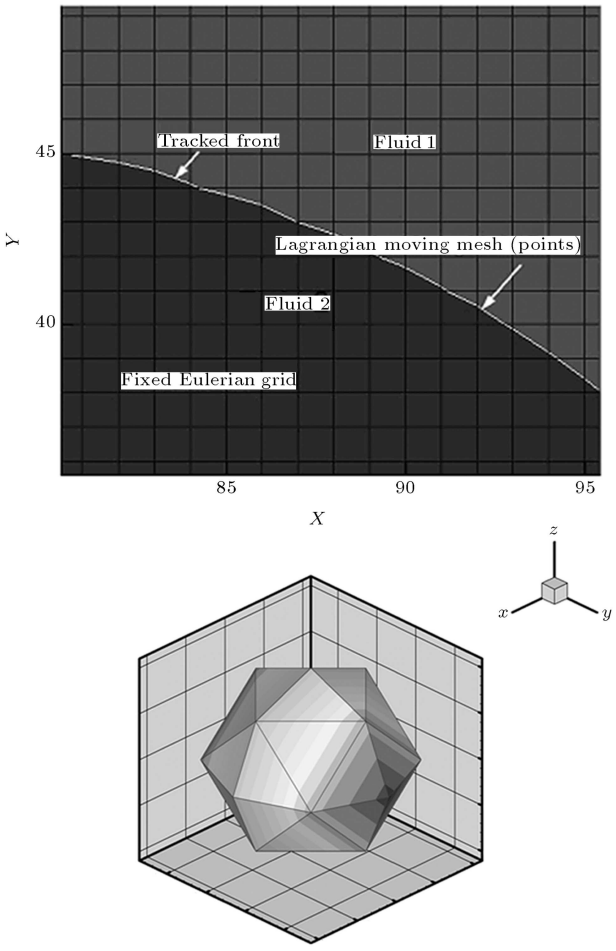

Figure 1. Eulerian and Lagrangian grids in hybrid front capturing and front tracking technique.

The procedure used for evaluation of the density and viscosity transport and the surface tension term is the key element in the numerical approach. In the Volume Of Fluid (VOF) approach, an indicator function is used to identify different phases of the flow. In the hybrid front capturing and front tracking approach, however, the interface is explicitly marked and tracked. Knowing the location of the front, the values of the fluid property at different flow locations are easily specified. However, identification of the moving front is associated with the following difficulties:

- How to best identify the front;
- How the data are transported between the fixed and moving grids;
- How the front moves with time;
- How to satisfy the conservation laws as the front shape changes during its motion.

In the present approach, as the front shape changes, some grid points are added or subtracted to maintain a proper grid for the front. Figure 2 shows a typical restructuring of the front grid. In the hybrid front capturing and front tracking approach when data is transferred between the two grids, it is very important that the conservation laws are satisfied. To advect the discontinuous density and viscosity fields, and to compute surface tension forces, the bubble surface is represented by separate computational elements, referred to as the front. The front grid is of one lower dimension than the stationary fluid grid and is advected by the fluid velocity which is interpolated from the fluid grid. To inject surface tension forces onto the fixed fluid grid, a technique that is usually called the Immersed Boundary Method and which was introduced by Peskin, is used. In this approach, the infinitely thin interface is approximated by a smooth distribution function which is used to distribute the surface forces over the grid points close to the surface in such a way that the total forces are conserved. Therefore, the front is given a finite thickness of about three to four grid spacings and there is no numerical diffusion of this front, since the thickness remains constant for all time. To generate the density and viscosity fields from the front, a technique introduced by Unverdi and Tryggvason [9] is used which is based on distributing the jump in these quantities onto the fixed grid by the Peskin technique and then solving a Laplace equation for the field variable itself.

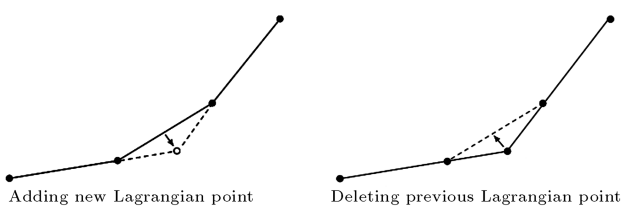

Figure 2. Restructuring of a Lagrangian grid.

For code verification purposes, the incompressible lid-driven cavity flow was simulated. Figure 3 shows the X-velocity component profile along the vertical centerline and the Y-velocity component profile along the horizontal for Re = 100, which, in comparison with the results of Ghia et al. [23], show very good agreement.

For a bubble under micro-gravity conditions, grid independency studies were also performed for 98×66, 146×98, and 194×130 grids. The related results are summarized in Figure 4. It is seen that, for the fist course grid, the shape of the bubble is distorted, but for the last two refined grids, the front shapes are roughly the same. Thus, the 146×98 grid was chosen for the sake of economy of the computations.

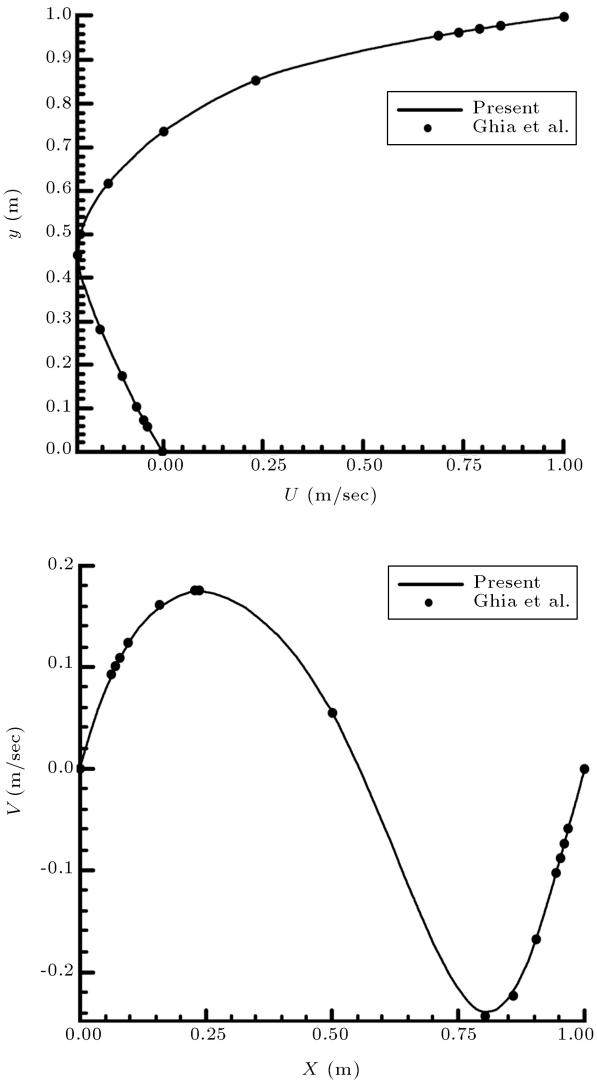

Figure 3. X- and Y- velocity components profiles at the centerline of the cavity.

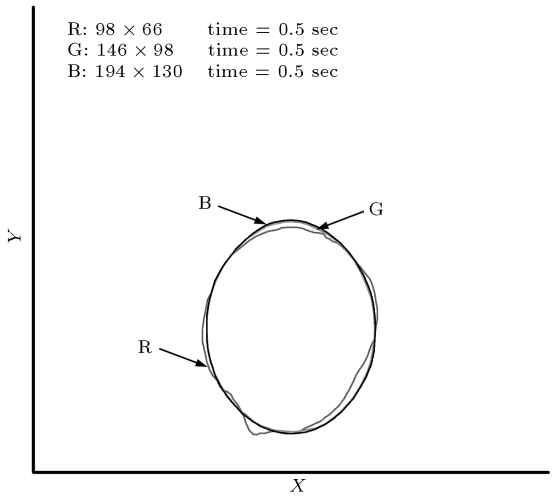

Figure 4. Grid independency study (case 2).

For a non-isothermal condition test case, the fluids consist of the same ideal gas held at a uniform temperature (T_i); the position of the membrane was R_i and the total mass of the gas in the enclosure was $\mathbf{m}$. Fluid B was heated adjacent to the walls by heat flux (q) for time t_0. The temporal evolution of the membrane radius is presented in Figure 5. The final state for this case is in good agreement with the exact theoretical solution. The transient behavior seems to evolve in three phases: First, the heated fluid, B, expands, causing a compression of fluid A and, thus, decreases the membrane radius. The pressure in fluid A rises until it exceeds that in B, upon which the membrane begins to re-expand. Once the heating ceases and the temperature in the enclosure begins to homogenize, the pressure in fluid B drops further, relative to that in fluid A, and the membrane continues to expand until it reaches a steady final value.

RESULTS AND DISCUSSIONS

In this work, the rising of a single bubble in a quiescent liquid under microgravity conditions was computationally simulated. In addition to general studies of microgravity effects, the initiation of hydrodynamic convection, solely due to the variations of interface curvature (surface tension force) and thus the generation of shearing forces at the interfaces, was also studied. Then, the variation of surface tension due to temperature (Marangoni convection) can initiate the onset of convection even in the absence of buoyancy studied. The results show that the bubble moves in a straight path under microgravity condition compared to the zigzag motion of bubbles in the presence of gravity. The related unsteady incompressible full Navier-Stokes equations were solved using a conventional finite difference method with a structured staggered grid. Also, a Multigrid technique in the context of the projection method improved convergences and computational stiffness. The interface was tracked explicitly by connected marker points via a hybrid front capturing and tracking method.

Multi-grid iteration combines classical iterative techniques, such as the Gauss-Seidel line or point relaxation with sub-grid refinement procedures to yield a method superior to the iterative techniques alone. By iterating and transferring approximations and corrections at sub-grid levels, a good initial guess and rapid convergence at the fine grid level can be achieved. Multiphase flow computations involve several challenging issues. For example, the momentum, mass and energy transfer between phases are coupled. When the interface moves, one needs to compute the domain shape and associated geometric information, such as curvature and normal and projected area/volume, as part of the solution which adds nonlinearity to the

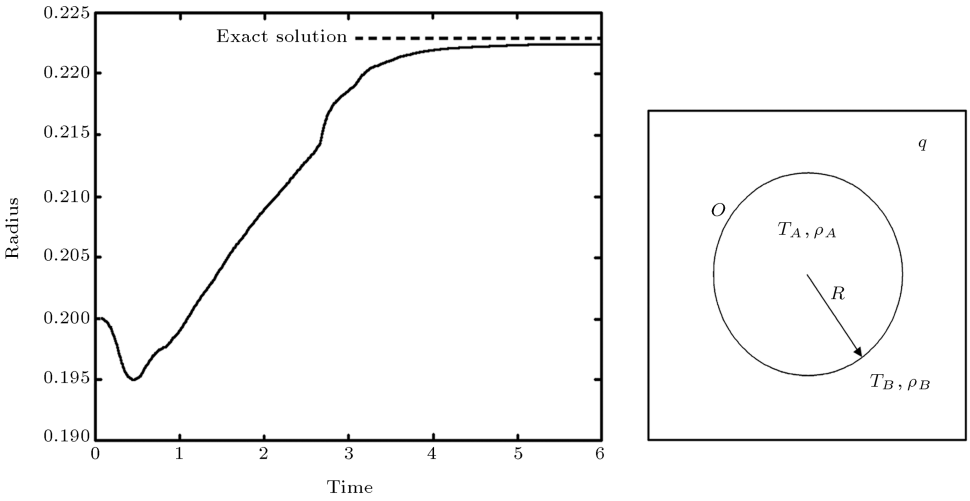

Figure 5. Temporal evolution of the membrane radius.

problem and can create difficulties in grid generation. Oftentimes, there are large property jumps across the interface, e.g. the density ratio between vapor and water under standard sea level conditions is around 1,000, which results in multiple time and length scales and computational stiffness. To deal with these issues, numerous numerical techniques have been developed, each with its own merits and difficulties. The present approach tracks the interface with the Lagrangian method using massless markers while the field equation computations are carried out with the Eulerian method on fixed Cartesian meshes. The pressure equation which is a diffusion-type for low speed flows, exhibits slower convergence rates than the convective-diffusive ones when employing iterative matrix solvers. Therefore, improvement on the solver of the Poisson equation can accelerate the overall performance of the method. The property jump between phases also alters the convergence behavior. In this study, the moving boundary separating two fluids and the effect of the property ratios between phases was used. The multi-grid technique works on the principle that high wave number components decay faster than low wave number components. A component's wave number is considered high or low, depending on the grid size. This dependence is such that low wave number components on a fine mesh behave like high wave number components on a coarse mesh. Therefore, treating the various wave number components on different grids makes it possible to accelerate the convergence rate.

Figure 6 shows typical bubble shapes in time for different density ratios; 10, 100. The initial bubble starts to rise due to the effect of buoyancy in the cylinder, and it eventually deforms to a steady-state shape. Figure 7 shows the number of fine grid iterations required to reach a residual level of 10^{-6}

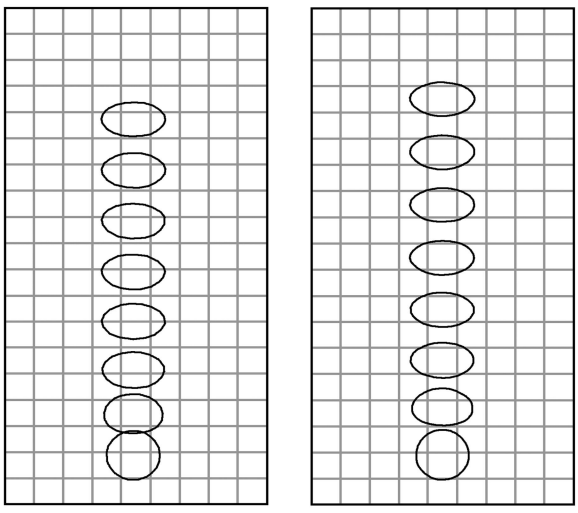

Figure 6. Bubble shapes evolution for different density ratios 10 (left) and 100 (right).

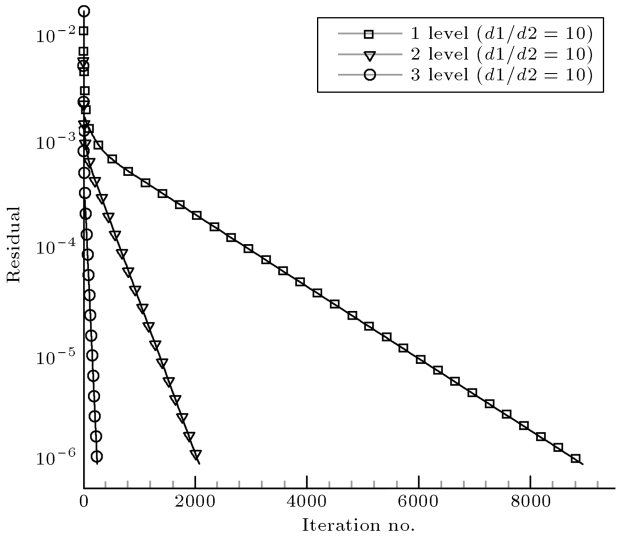

Figure 7. Residual history for different levels.

at the very first time step, which requires the largest number of iterations to converge among all time steps, since it starts to iterate from initial conditions; one level represents the iteration history for a single grid computation. As demonstrated, the convergence rate improves dramatically when the level of the multi-grid is increased.

Different cases studied (for isothermal rising) are listed in Table 2. The selected simulation conditions are such that the bubble motion is under low or zero gravity. Different cases have been introduced in order to study both the buoyancy and hydrodynamic convection effects. According to Table 1, the bubble shape varies from spherical to ellipsoidal (or equivalent shape in 2 dimensions), for different Reynolds and Bond numbers. Also, depending on these shapes, the bubble follows a straight line or zigzag curve while moving upward.

The evolutions of the pressure and density fields are shown in Figure 8. The unsteady motion of the bubble is clearly shown in this figure.

Figure 6 shows the bubble shape evolution from circular at the initial stage to elliptical at later times, while following a straight path. Note that in cases 1, and 3, in the absence of gravity, the motion is only due to the curvature induced lift force given as:

$$\text{Lift} = \sigma kn\delta(X - X^f). \tag{16}$$

This lift force is due to the surface tension coefficient and interfacial curvature. However, for the initial cylindrical bubble, the value of this force is zero and, thus, its onset is due to an initial disturbance. It should be noted that a similar phenomenon, entitled "parasitic currents", has been reported especially for gas-liquid interfaces. Parasitic currents are unphysical currents generated in using implementations of the Continuum

Table 2. Different test cases considered in this study.

Case No.	Surface Tension (N/m)	Gravity (m/s^2)	Reynolds Number (Re_B)	Bond Number (Eo)	Morton Number (Mo)	Weber Number (We)	Froude Number (Fr)
1	0.2	0	800	0	0	800	∞
2	0.2	0.06	800	0.048	7.5×10^{-8}	800	16666
3	0.5	0	2000	0	0	320	∞
4	0	0	800	0	-	∞	∞

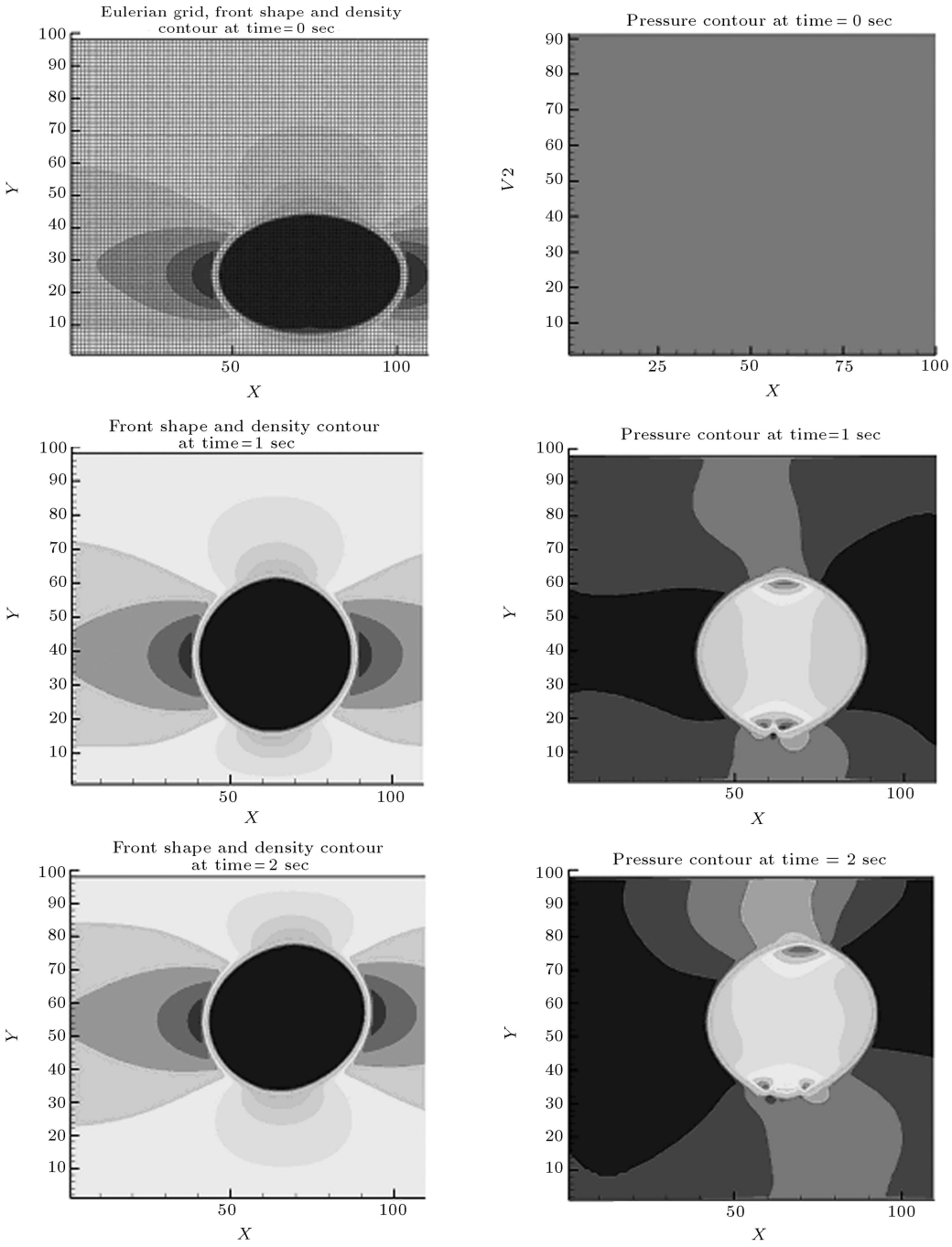

Figure 8. Density (left) and pressure (right) shadowgraphs of bubble motion in a quiescent liquid under zero gravity condition (case 3).

Surface Force (CSF) technique to model surface tension forces in multi-phase computational fluid dynamics problems. However, this phenomenon has a limited magnitude regarding fluid properties [24]. Also, in our computational methodology, the CSF scheme has not been used. Then, it seems that some parts of this hydrodynamic convection can exist physically. Equation 16 shows that changes in the curvature or in the surface tension coefficient can initiate bubble motion, even in the absence of gravity. Here, the surface tension coefficient is constant (since there is no temperature gradient). Thus, the only driving force for the bubble motion is the variation in the shape of the interface and initial disturbance. Figure 9 shows the evolution of the shape of the bubble with time.

The results for case 2 are shown in Figure 10. As shown in this figure, when gravity is low, the buoyancy and the hydrodynamic forces tend to move the bubble. The resulting lift force is given as:

$$\text{Lift} = \rho g + \sigma k n \delta (X - X^f). \tag{17}$$

As expected from this figure, the bubble movement is faster here, compared to case 1.

Figure 11 shows the results related to case 3, where the surface tension coefficient is higher, but still, gravity is set to zero. Note from this figure that the bubble has higher upward velocity in comparison with the results of case 1 where the surface tension coefficient was lower. The driving force for the bubble motion in this case is the hydrodynamic convection effect caused by the changes in the bubble curvature. This force is larger than the driving force of case 1 due to a higher surface tension coefficient.

Figure 12 shows the results of case 4 where both surface tension and gravity are zero. According to Equation 17, the lift force is zero and, thus, there is

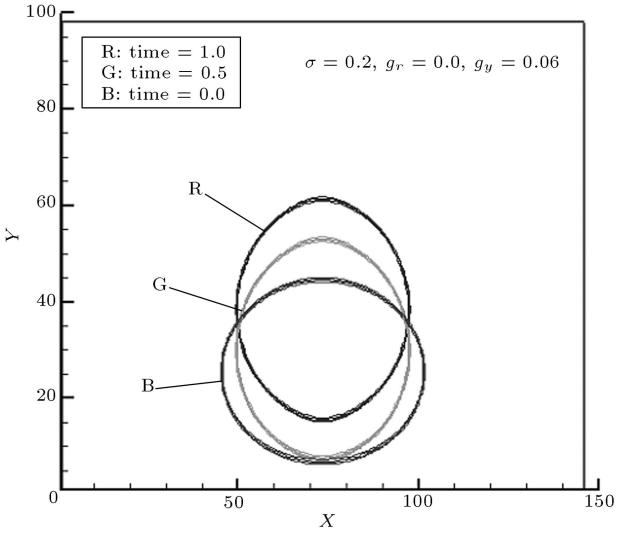

Figure 9. Bubble evolution (case 1).

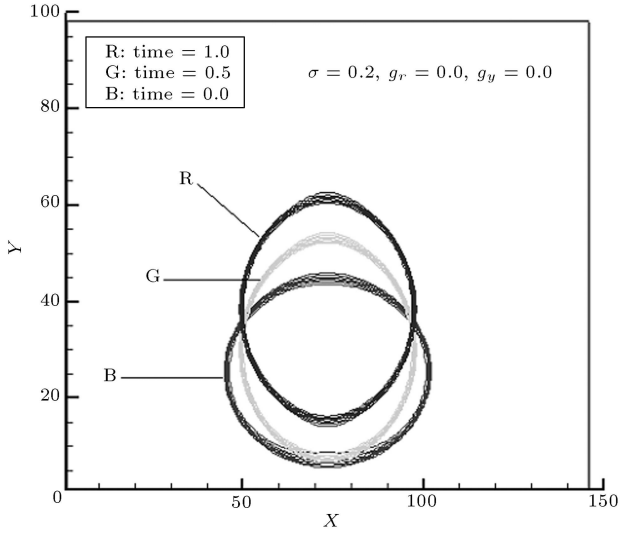

Figure 10. Bubble evolution (case 2).

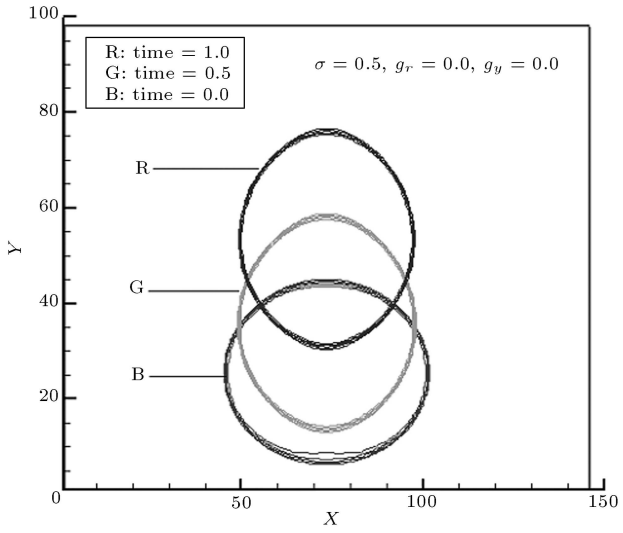

Figure 11. Bubble evolution (case 3).

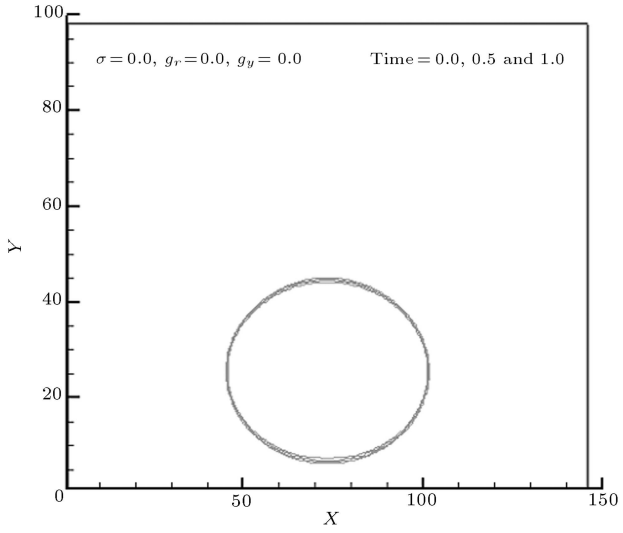

Figure 12. Bubble evolution (case 4).

no bubble motion with time which is consistent with the results of Figure 12.

In Figure 13, cases 1, 3 and 4 are compared for $t = 1$ second. Note that in the absence of gravity, the higher the surface tension coefficient is, the higher is the upward lift force that leads to a higher bubble velocity. Also, as shown in this figure, higher surface tension coefficient causes a higher upward motion of the bubble.

The results of case 1, at longer times, are shown in Figure 14. The important point in this figure is that the bubble has a downward motion at $t = 2$ seconds. Here, the change in the direction of motion is due to the change in the sign of the lift force caused by changes in the bubble curvature (hydrodynamic convection effect).

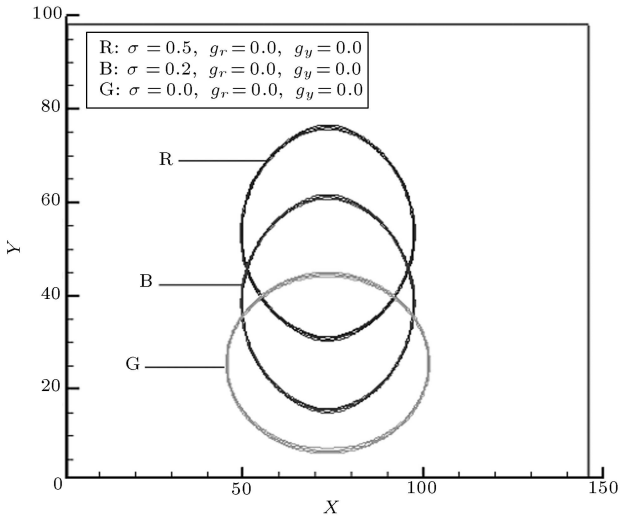

Figure 13. The comparison of Marangoni force (cases 1, 2 and 4) at $t = 1$ sec.

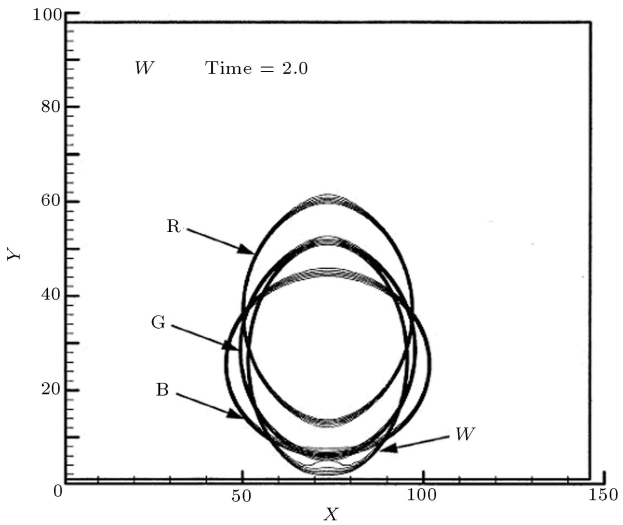

Figure 14. Bubble evolution (case 1) showing negative lift at $t = 2$ second.

The evolutions of the temperature fields are shown in Figure 15 under zero gravity conditions. The unsteady motion of the bubble is clearly shown in this figure. Also, Isotherms (right) and Flow field (left) for a bubble under micro gravity are shown in Figure 16. Another characteristic feature of Marangoni convection becomes obvious from the numerical simulation with an existing temperature gradient, i.e. this convection tends to reduce its driving temperature difference. With the growing intensity of the Marangoni convection, i.e. growing Marangoni number, the temperature gradient along the interface is more and more reduced. As shown in Figures 15 and 16, the number

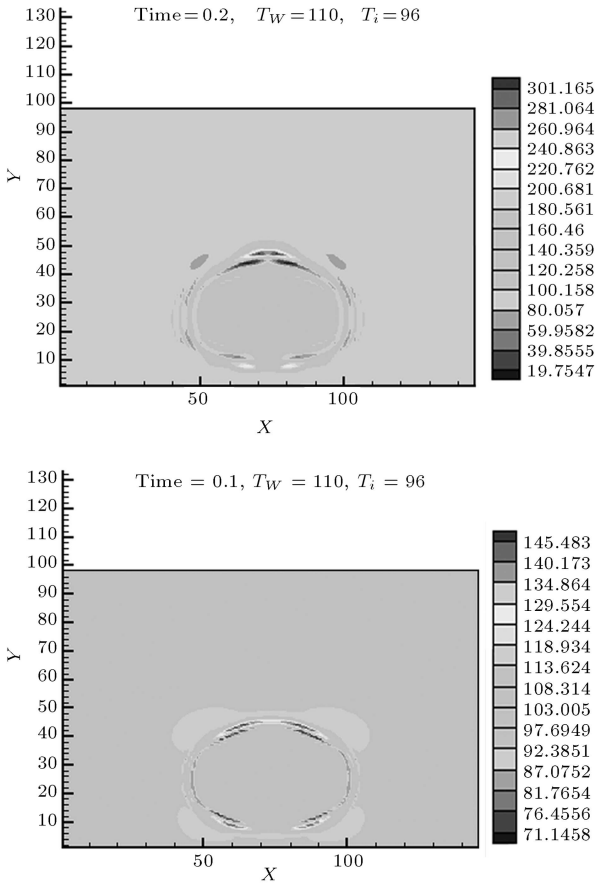

Figure 15. Temperature shadowgraphs of bubble motion in a quiescent liquid under zero gravity condition (initial temperature = 96, wall temperature = 110).

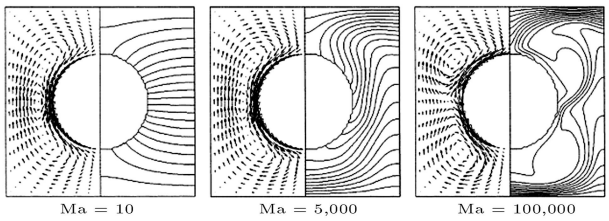

Figure 16. Isotherms (right) and flow field (left) for a bubble under micro gravity.

of isotherms touching the bubble surface decreases with the increasing intensity of the flow. Even for the smallest temperature differences along the bubble interface, i.e. small Marangoni numbers, a fluid motion with a typical toroidal vortex can be observed. In contrast to buoyancy convection, no critical Marangoni number has to be reached for the onset of fluid flow. With a growing Marangoni number, the isotherms are displaced from the bubble towards the rigid surfaces, leading to an increased heat transfer there.

CONCLUSIONS

In this work, large bubble motion in a quiescent liquid is computationally simulated by a hybrid front capturing and front tracking method. The main conclusions are as follows:

- For all cases studied here (for the values of the dimensionless numbers studied), the bubble moves in a straight path, which is in contrast with the bubble motion under normal gravity conditions.
- At microgravity conditions, the driving force for the bubble motion (isothermal) is the variation in the bubble surface curvature. Both the buoyancy and hydrodynamic convection effects create positive lift and thus tend to move the bubble upward. However, this trend continues up to the point where the lift force changes in direction and thus the bubble moves downward.
- As the density ratio increases, the number of iterations required to reach the same residual level also increases. The multi-grid technique, in the context of the projection method, improved convergences and computational stiffness.
- With growing Marangoni number (for non-isothermal cases), the isotherm lines are displaced from the bubble towards the rigid surfaces, leading to an increased heat transfer there.

NOMENCLATURE

V	bubble volume
$\mathbf{g}$	gravitational acceleration
r_{eq}	equivalent radius
U_T	terminal velocity
$\mathbf{u}$	velocity vector field
σ	surface tension coefficient
$\mathbf{n}$	normal unit vector at interface
k	interfacial curvature
P	pressure
ν	kinematic viscosity coefficient
δ	Dirac delta function
H	Heaviside function
x^f, y^f	coordinates of nodes in moving grid
x, y	coordinates of nodes in fixed grid
A	the bubble surface area
T	temperature
c_p	specific heat
c_1	specific heat (primary phase)
c_2	specific heat (secondary phase)
$\dot{m}_f$	interfacial mass transfer
k'	conductive coefficient
L_0	latent heat

REFERENCES

1. Unverdi, S.O. and Tryggvason, G. "Computations of multi-fluid flows", *Physica. D 60*, pp. 70-83 (1992).
2. Brackbill, J.U., Kothe, D.B., and Zemach, C. "A continuum method for modeling surface tension", *J. Comput. Phys.*, **100**, pp. 335-354 (1992).
3. Sussman, M., Smereka, P. and Osher, S. "A level set approach for computing solutions to incompressible two-phase flows", *J. Comput. Phys.*, **114**(1), pp. 146-159 (1994).
4. Ryskin, G. and Leal, L.G. "Numerical solution of free-boundary problems in fluid mechanics. Part 2. Buoyancy-driven motion of a gas bubble through a quiescent liquid", *J. Fluid Mech.*, **148**, pp. 19-35 (1984a).
5. Dandy, D.S. and Leal, G.L. "Buoyancy-driven motion of a deformable drop through a quiescent liquid at intermediate Reynolds numbers", *J. Fluid Mech.*, **208**, pp. 161-192 (1989).
6. Kang, I.S. and Leal, L.G. "Numerical solution of axisymmetric, unsteady free-boundary problems at finite Reynolds number. I. Finite-difference scheme and its applications to the deformation of a bubble in a uniaxial straining flow", *Phys. Fluids*, **30**(7), pp. 1929-1940 (1987).
7. Oran, E.S. and Boris, J.P. "Numerical simulation of reactive flows", *Elsevier*, New York, 1st Ed. (1987).
8. Glimm, J. "Nonlinear and stochastic phenomena: The grand challenge for partial differential equations", *SIAM Review*, **33**, pp. 625-643 (1991).
9. Unverdi, S.O. and Tryggvason, G. "A front-tracking method for viscous, incompressible multi-fluid flows", *J. of Comput. Phys.*, **100**, pp. 25-37 (1992).
10. Loth, E., Taebi-Rahni, M. and Tryggvason, G. "Deformable bubbles in a free shear layer", *Int. J. Multiphase Flow*, **23**(5), pp. 977-1001 (1997).
11. Loth, E., and Taebi-Rahni, M. "Forces on a large cylindrical bubble in an unsteady rotational flow", *AIChE Journal*, **42**(3), pp. 638-648 (1996).

12. Loth, E., Taebi-Rahni, M. and Tryggvason, G. "Flow modulation of a planar free shear layer with large bubbles-direct numerical simulations", *Int. J. Multiphase Flow*, **20**(6), pp. 1109-1128 (1994).
13. Nobari, M.R., Jan, Y.J. and Tryggvason, G. "Head-on collision of drops", *Phys. Fluids*, **8**, pp. 29-42 (1996).
14. Han, J. "Numerical studies of drop motion in axisymmetric geometry", PhD. Dissertation, Mech. Eng. Department, the University of Michigan, Ann Arbor, MI, USA (1998).
15. Adams, J. "Multigrid software for elliptic partial differential equations: MUDPACK", *NCAR Technical Note-357*, pp. 51-72 (1991).
16. Press, W.H., Teukolsky, S.A., Vetterling, W.T. and Flannery, B.P., *Numerical Recipes in Fortran, the Art of Scientific Computing*, 2nd Ed., Cambridge University Press, London (1992).
17. Shyy, W., Francois, M., Udaykumar, H.S. and Tran-Son-Tay, R. "Moving boundary in micro-scale biofluid dynamics", *Applied Mechanics Reviews*, **54**, pp. 419-53 (2001).
18. Vries, A.W. "Path and wake of a rising bubble", PhD Dissertation, Mech. Eng. Department, Twent University, Netherlands (2001).
19. Han, Y.Y., Seiichi, K. and Yoshiaki, O. "Direct calculation of bubble growth, departure, and rise in nucleate pool boiling", *Int. J. of Multiphase Flow*, **27**, pp. 277-298 (2001).
20. Peskin, C.S. and Fauci, L.J. "A computational model of aquatic animal locomotion", *J. Computational Physics*, **77**, p. 85 (1988).
21. Esmaeeli, A. and Tryggvason G. "Direct numerical simulation of bubbly flows", *J. Fluid Mech.*, **37**, pp. 313-345 (2001).
22. Shin, S. and Juric, D. "Modeling three-dimensional multiphase flow using a level contour reconstruction method for front tracking without connectivity", *J. of Computational Physics*, **180**, pp. 427-470 (2002).
23. Ghia, U., Ghia, K.N. and Shin, C.T. "High Resolutions for incompressible flow using the Navier-Stokes equations and a multigrid method", *J. Comp. Physic*, **48**, pp. 387-411 (1982).
24. Harvie, D.J., Davidson, M.R. and Rudman, M. "An analysis of parasitic current generation in volume of fluid simulations", *J. Anziam*, **46**(E), pp. C133-C149 (2005).